

# Direct observational evidence for a large transient galaxy population in groups at $0.85 < z < 1$

Michael L. Balogh<sup>1</sup>, Sean L. McGee<sup>1,2</sup>, David J. Wilman<sup>3</sup>, Alexis Finoguenov<sup>3,4</sup>, Laura C. Parker<sup>5</sup>, Jennifer L. Connelly<sup>3</sup>, John S. Mulchaey<sup>6</sup>, Richard G. Bower<sup>2</sup>, Masayuki Tanaka<sup>7</sup>, Stefania Giodini<sup>8</sup>

<sup>1</sup>*Department of Physics and Astronomy, University of Waterloo, Waterloo, Ontario, N2L 3G1, Canada*

<sup>2</sup>*Department of Physics, University of Durham, Durham, UK, DH1 3LE*

<sup>3</sup>*Max-Planck-Institut für extraterrestrische Physik, Giessenbachstrasse 85748 Garching Germany*

<sup>4</sup>*CSST, University of Maryland, Baltimore County, 1000 Hilltop Circle, Baltimore, MD 21250, USA*

<sup>5</sup>*Department of Physics and Astronomy, McMaster University, Hamilton, Ontario, L8S 4M1 Canada*

<sup>6</sup>*Observatories of the Carnegie Institution, 813 Santa Barbara Street, Pasadena, California, USA*

<sup>7</sup>*Institute for the Physics and Mathematics of the Universe, University of Tokyo, Kashiwa 2778582, Japan*

<sup>8</sup>*Leiden Observatory, Leiden University, PO Box 9513, 2300 RA Leiden, the Netherlands*

11 January 2011

## ABSTRACT

We introduce our survey of galaxy groups at  $0.85 < z < 1$ , as an extension of the Group Environment and Evolution Collaboration (GEEC). Here we present the first results, based on Gemini GMOS-S nod-and-shuffle spectroscopy of seven galaxy groups selected from spectroscopically confirmed, extended *XMM* detections in COSMOS. We use photometric redshifts to select potential group members for spectroscopy, and target galaxies with  $r < 24.75$ . In total we have over 100 confirmed group members, and four of the groups have  $> 15$  members. The dynamical mass estimates are in good agreement with the masses estimated from the X-ray luminosity, with most of the groups having  $13 < \log M_{\text{dyn}}/M_{\odot} < 14$ . We compute stellar masses by template-fitting the spectral energy distributions; our spectroscopic sample is statistically complete for all galaxies with  $M_{\text{star}} \gtrsim 10^{10.1} M_{\odot}$ , and for blue galaxies we sample masses as low as  $M_{\text{star}} \sim 10^{8.8} M_{\odot}$ . The fraction of total mass in galaxy starlight spans a range of 0.25–3 per cent, for the six groups with reliable mass determinations. Like lower-redshift groups, these systems are dominated by red galaxies, at all stellar masses  $M_{\text{star}} > 10^{10.1} M_{\odot}$ . Few group galaxies inhabit the “blue cloud” that dominates the surrounding field; instead, we find a large and possibly distinct population of galaxies with intermediate colours. The “green valley” that exists at low redshift is instead well-populated in these groups, containing  $\sim 30$  per cent of the galaxies. These do not appear to be exceptionally dusty galaxies, and about half show prominent Balmer-absorption lines. Furthermore, their *HST* morphologies appear to be intermediate between those of red-sequence and blue-cloud galaxies of the same stellar mass. Unlike red-sequence galaxies, most of the green galaxies have a disk component, but one that is smaller and less structured than disks found in the blue cloud. We postulate that these are a transient population, migrating from the blue cloud to the red sequence, with a star formation rate that declines with an exponential timescale  $0.6 \text{ Gyr} < \tau < 2 \text{ Gyr}$ . Such galaxies may not be exclusive to the group environment, as we find examples also amongst the non-members. However, their prominence among the group galaxy population, and the marked lack of blue, star-forming galaxies, provides evidence that the group environment either directly reduces star formation in member galaxies, or at least prevents its rejuvenation during the normal cycle of galaxy evolution.

**Key words:** galaxies: clusters

## 1 INTRODUCTION

Galaxy evolution since about  $z \sim 2$  is characterized generally by the cessation of star formation. On average, the star

formation rate density in the Universe has declined by a factor  $\sim 10$  since that time (e.g. Lilly et al. 1996; Hopkins 2004; Gilbank et al. 2010). The rate of decline appears to depend on both stellar mass (e.g. Cowie et al. 1996; Juneau et al. 2005; Noeske et al. 2007; Bell et al. 2007; Gilbank et al. 2010) and environment (e.g. Poggianti et al. 2006; Cooper et al. 2008; Maier et al. 2009; Iovino et al. 2010; Vulcani et al. 2010; Peng et al. 2010; Cucciati et al. 2010; Sobral et al. 2010; McGee et al. 2010). This leads to a fairly consistent empirical description, at least for massive galaxies. The galaxy population is well-modeled by having star formation “quenched” on relatively short timescales; this quenching happens first for the most massive galaxies, and later for lower-mass systems (e.g. Noeske et al. 2007). This evolution is somewhat accelerated in denser environments (Iovino et al. 2010; Vulcani et al. 2010; Li et al. 2010), especially for the lowest-mass galaxies studied to date.

However, we lack a clear understanding of the physical processes driving this evolution. It appears that the dependence on stellar-mass and environment are separable (Baldry et al. 2006), and likely point to different mechanisms. Recently, Peng et al. (2010) have proposed an interesting empirical description of this, where the quenching rate is described by one term that is proportional to star formation rate, and another that is related to the local density. This works surprisingly well, but still doesn’t lend itself to a clear physical interpretation.

Galaxy formation models are too complex and under-constrained to provide an unequivocal answer at this time. However, they do indicate that parametric treatments of energy input due to supernova and supermassive black hole accretion can do a reasonable job of explaining the mass-dependent quenching (e.g. Croton et al. 2006; Bower et al. 2008). The environmental term is accounted for to some extent in the so-called “halo model”, where the central galaxy of a given dark matter halo is treated somehow differently from the satellites (e.g. Gilbank & Balogh 2008; Skibba & Sheth 2009; McGee et al. 2009). Such a distinction is expected at some level, since the hot gas that is thought to fill a common halo should, for the most part, cool and condense only onto the central galaxy. Much of the hot gas associated with satellite galaxies will likely get tidally stripped, ram-pressure stripped, or shock heated until it becomes part of the common halo (e.g. McCarthy et al. 2008; Kawata & Mulchaey 2008; Font et al. 2008). This picture relies on a number of untested assumptions, however, and simple implementations of this do not do a very good job of predicting the observed star formation histories of grouped galaxies (Weinmann et al. 2006; Gilbank & Balogh 2008; Balogh et al. 2009).

The study of galaxy evolution in dense environments has been hampered by several observational difficulties. The easiest place to look is in the cores of rich clusters at relatively low redshift (e.g. Balogh et al. 1997; Poggianti et al. 1999; Balogh et al. 2002; Lewis et al. 2002; Gomez et al. 2003; Lu et al. 2009, and many others). But the cores of rich clusters are extreme environments where, for example, ram-pressure stripping can remove even the cold gas from disks (e.g. Quilis et al. 2000; Koopmann & Kenney 2004), and galaxy interactions effectively distort galaxy morphologies (Moore et al. 1996). These are interesting processes, but are unlikely to be the explanation for trends observed in lower-density environments (e.g. Balogh et al. 2004). Moreover, low redshift systems provide additional challenges. Galaxies at low redshift are generally older and more gas poor, due to normal evolution, so there is less potential for environment to disrupt star formation. Also, the accretion rate of new, relatively gas-rich galaxies, into

clusters is lower than it was in the past (e.g. Ellingson et al. 2001; McGee et al. 2009), and recently accreted galaxies will represent a small fraction of the entire population which has built up over a Hubble time. So there is less opportunity to catch galaxies in the act of transformation, if such a process occurs.

Thus, the best place to observe environmentally-driven evolution in action is in gas-rich, low-mass galaxies inhabiting small groups, at relatively high redshift. This was the motivation behind the Group Environment and Evolution Collaboration (GEEC), that began with deep Magellan LDSS3 spectroscopy of groups at  $0.3 < z < 0.55$ , selected from the CNOC2 survey fields (Wilman et al. 2005a,b). In a series of papers we showed that while disk-dominated, star forming galaxies of a given stellar mass are less common in groups than in the general field, the properties of the star-forming population itself seems independent of environment (e.g. McGee et al. 2010). This is surprising, as it suggests that either the transformation is very rapid, or the number of galaxies undergoing transformation at the epoch of observation is small. At the same time, group galaxies look much more like the general field in most respects than is the case at lower redshift (McGee et al. 2010). This suggests that evolution in groups is a relatively recent phenomenon (see also Lu et al. 2009).

Nonetheless, groups at  $z \sim 1$  and beyond still show a larger population of passively-evolving galaxies than the surrounding field (e.g. Cooper et al. 2010). Interestingly, however, there is increasing evidence that those galaxies that *are* forming stars, are doing so at a higher rate than field galaxies of similar stellar mass (Elbaz et al. 2007; Muzzin et al. 2008; Cooper et al. 2008; Ideue et al. 2009; Sobral et al. 2010; Li et al. 2010; Kocevski et al. 2010). It may be at this epoch that dense environments stimulate star formation, leading to a rapid consumption of gas and leading to the dominant old population at  $z = 0$ . The joint density- and mass-dependence of this effect is nicely illustrated by Sobral et al. (2010). The higher accretion rate, and younger age of the Universe, has led us to predict that there will be more diversity among galaxy groups at this redshift (McGee et al. 2009).

We have thus embarked on an ambitious spectroscopic campaign, using the GMOS spectrographs on Gemini North and South to study the galaxy populations in  $\sim 20$  groups, mostly selected within the COSMOS (Scoville et al. 2007b) survey fields. The deep spectroscopy achieves two main goals. First, we can study galaxies with low stellar mass; our sample is complete for *red* galaxies 1.0 mag fainter than the zCOSMOS 10k survey (Lilly et al. 2007), 0.65 mag fainter than DEEP2 (Cooper et al. 2008) and  $\sim 0.25$  mag fainter than EDisCS at this redshift (Halliday et al. 2004); for blue galaxies we are complete to even fainter magnitudes. This depth is vital for studying environmental effects, which appear to be most important for the lowest-mass galaxies (Cucciati et al. 2010). Secondly, the depth allows us to obtain  $\sim 20$  spectroscopic members per group, which is sufficient to estimate the dynamical mass, and dynamical state, of each group (Hou et al. 2009). Moreover, it allows us to consider the galaxy population of individual groups, or subsets of groups. Thus, we can attempt to link transient galaxies to the dynamics or recent accretion history of the larger-scale environment.

We present our data, including a full description of the group and spectroscopic selection, in § 2. The basic analysis of redshift and stellar mass measurements, and determination of group dynamical masses, is presented in § 3. Our main results, on the stellar fraction and the discovery of a dominant group population of galaxies with intermediate colours, spectral type and morphology, are pre-

sented in § 4. Finally, we discuss the implications of our results, and summarize our conclusions, in § 5.

Throughout the paper, we assume a cosmology with  $\Omega_m = 0.3$ ,  $\Omega_\Lambda = 0.7$  and  $h = H_0 / (100 \text{ km/s/Mpc}) = 0.7$ . All magnitudes are on the AB system.

## 2 DATA

### 2.1 The parent catalogues

Our survey targets galaxy groups within the COSMOS field (Scoville et al. 2007b). This field benefits from a wide range of publicly available, deep, multiwavelength photometry. The backbone is the widest *Hubble Space Telescope* (HST) survey ever undertaken, covering  $\sim 2$  square degrees with the F814W filter on the *Advanced Camera for Surveys* (Scoville et al. 2007a). In addition, we will make use of the deep X-ray observations obtained with *XMM* (Hasinger et al. 2007) and *Chandra* (Elvis et al. 2009);  $3.6\mu\text{m} - 24\mu\text{m}$  data from *Spitzer* IRAC and MIPS (Sanders et al. 2007), and ground-based optical and near-infrared photometry from a variety of sources (Capak et al. 2007).

Our survey is built on three important contributions to COSMOS. First are the exquisite photometric redshifts, derived from the photometry of 30 broad, intermediate and narrow-band filters (Ilbert et al. 2009). These are derived using a template-fitting technique, and calibrated based on large spectroscopic samples. Even for the faintest galaxies in our sample, most of the objects have photometric redshifts determined to better than 10 per cent (see § 2.3.1). Secondly, we use the 10K release of the zCOSMOS spectroscopic survey (Lilly et al. 2007, 2009), from which we obtain redshifts for moderately bright galaxies ( $I_{AB} < 22.5$ ) over most of the survey area. This is a sparsely-sampled redshift survey, with  $\sim 40$  per cent sampling completeness.

The third pillar of our survey comes from analysis of the deep X-ray data (Finoguenov et al. 2007). Using an established wavelet technique (e.g. Finoguenov et al. 2009, 2010) it has become possible to detect extended X-ray emission from groups of galaxies out to  $z \sim 1$ . Identification of group redshifts is done using all available spectroscopy, including but not limited to the 10K zCOSMOS survey. The combination of X-ray and redshift data provides a robust catalogue of groups and clusters, to enable follow-up (Finoguenov et al., in prep). Masses are estimated from X-ray scaling relations (e.g. Rykoff et al. 2008), and calibrated from a stacked weak-lensing analysis (Leauthaud et al. 2010). Catalogues based on redshift only (e.g. Gerke et al. 2005; Knobel et al. 2009) are powerful tools with which to probe the evolution in the average properties of groups. However, such catalogues suffer from contamination and projection effects which make it difficult to interpret studies of individual systems. The cross-correlation with X-ray allows one to obtain a more robust sample of groups. This potentially introduces a scientifically interesting bias, if groups with X-ray emission have fundamentally different populations from groups of similar mass without such emission. However, the main difference between optically- and X-ray-selected samples seems to be primarily just that the latter preferentially selects more massive systems (Jeltema et al. 2009; Finoguenov et al. 2009; Balogh et al. 2010). We thus use this catalogue as the basis of our group selection, which we describe in the following subsection.

### 2.2 Galaxy group selection

For our survey, we are interested in the lowest-mass groups that are robustly identified, and within the redshift range  $0.85 < z < 1$ . We considered all groups in the Finoguenov et al. (in prep) catalogue, that lie within this redshift range, have at least 3 spectroscopically-determined members, and were considered secure identifications. Specifically, we consider groups that are either category 1 (good detection, with a well-determined X-ray centre) or category 2 (secure detection, but with an unreliable X-ray centre). There are 21 groups satisfying this selection. Of these, we have given preference to the lowest-mass, highest redshift systems, and have avoided targets that already have  $> 10$  redshifts used in the identification. The latter selection is made in part to avoid massive clusters, and to ensure our spectroscopy increases the total number of groups in the field with large, spectroscopically-confirmed membership.

Our first observations, described in § 2.3, targeted six of these groups. Their properties are tabulated in Table 1.

### 2.3 Gemini Observations

#### 2.3.1 Spectroscopic target selection

A crucial part of our strategy is the use of photometric redshifts to select potential group members. We give highest priority to galaxies that have  $21.5 < r < 24.75$ , and a redshift within  $2\sigma_{zphot}$  of the estimated group redshift, where  $\sigma_{zphot}$  is the 68 per cent confidence level on the photometric redshift<sup>1</sup>. Secondary priority slits are allocated to galaxies with  $15 < r < 24.75$  and  $0.7 < z_{phot} < 1.5$ .

We designed 3–4 GMOS masks on each target, using the GMPS software. On each mask we are able to allocate 40–50 slits. Typically, well over half the slits on the first mask are allocated to our top priority objects. This fraction decreases on subsequent masks, as we use up these targets. In most cases, with three masks we are able to target at least 40 of these high priority galaxies. All masks for a given target use the same alignment stars and are at the same position angle; thus a small fraction of the CCD area is unusable regardless of the number of masks obtained.

#### 2.3.2 Observations

We obtained 40 hours worth of observations on Gemini South, in the Band 1 queue during semester 10A. This returned science data of 2 hours on-source exposure, for 14 masks in 5 fields, covering six groups (two of the groups are located within the same GMOS field). All science observations were obtained in clear conditions with seeing 0.8 arcsec or better in  $i$ . The number of masks actually observed is given in Table 1.

The spectroscopy was obtained in nod & shuffle mode (Glazebrook & Bland-Hawthorn 2001), nodding the telescope by  $\pm 0.725$  arcsec from the centre of the slit, every 60s. This places the galaxy at the lower end of the 3 arcsec slit half the time, and at the upper end the other half of the time. We used microshuffling mode, so charge was shuffled by 21 pixels (3.05 arcsec). Four exposures

<sup>1</sup> At our redshift of interest, the average uncertainty on  $z_{phot}$  increases from  $\sigma_{zphot} \sim 0.007$  for the brightest galaxies to  $\sigma_{zphoto} \sim 0.04$  for those at our limit of  $r = 24.75$ . Even for these faintest objects, 90 per cent of the galaxies have  $z_{phot}$  uncertainties of less than  $\sigma_{zphot} < 0.07$ .

Group	RA deg (J2000)	Dec	$z_{\text{med}}$	$N_{\text{mask}}$	$N_{\text{mem}}$	$\sigma$ (km/s)	$R_{\text{rms}}$ Mpc	$M_{\text{dyn}}$ ( $10^{13} M_{\odot}$ )
40	150.41991	1.85265	0.97225	2	16	$765 \pm 124$	$0.32 \pm 0.03$	$12.84 \pm 5.50$
130	150.02586	2.20367	0.93828	3	26	$403 \pm 48$	$0.63 \pm 0.06$	$7.12 \pm 2.40$
134	149.65073	2.20932	0.94729	3	21	$384 \pm 60$	$0.92 \pm 0.07$	$9.44 \pm 3.69$
150	149.97472	2.31654	0.93428	4	20	$209 \pm 31$	$0.75 \pm 0.07$	$2.29 \pm 0.90$
161	149.95776	2.34531	0.94330	4	9	$372 \pm 56$	$0.45 \pm 0.07$	$4.36 \pm 2.01$
213	150.39697	2.49136	0.87990	2	7	$281 \pm 120$	$0.70 \pm 0.07$	$3.85 \pm 3.69$
213a	150.42715	2.49992	0.92650	2	6	$44 \pm 17$	$0.49 \pm 0.10$	-

**Table 1.** Properties of the seven galaxy groups observed with GMOS in semester 10A. The position, median redshift  $z_{\text{med}}$ , velocity dispersion, and the number of group members are determined from our GMOS spectroscopy (combined with available zCOSMOS 10k data), as described in the text. The number of GMOS masks observed in each field is given by  $N_{\text{mask}}$ ; note that groups 150 and 161 lie within the same field, as do groups 213 and 213a (a serendipitous discovery in the background).  $R_{\text{rms}}$  is the rms projected distance of all group members from the centre. The dynamical mass is computed as described in the text, from  $\sigma$  and  $R_{\text{rms}}$ . We do not compute a mass for group 213a, since the velocity distribution is unresolved and the membership is poor.

of 30 min each were taken, with small dithers in the spectral direction for the purpose of removing bad pixels and interpolating over the chip gaps.

Slits were 1 arcsec wide, and we use the R600 grism with OG515 order blocking filter. The detector was binned  $2 \times 2$ , resulting in a pixel scale of 0.146 arcsec/pix, and a dispersion of 0.93Å/pix. The resulting spectral resolution is limited by the slit width,  $\sim 6.4\text{\AA}$ .

Science observations were interspersed with GCAL flats. Calibration exposures for each mask consisted of CuAr arc lamp observations and twilight flats. In addition, we observed the standard star LTT6248 with a 1 arcsec, long slit, for flux calibration.

### 2.3.3 Data reduction

All data were reduced in IRAF, using the GEMINI packages with minor modifications. Slits were first identified from the GCAL flat exposures. A bad pixel mask was created using the routine GBPM, and a set of six long- and three short-exposure image flats. Pixels in the chip gaps, and outside the spectroscopic field of view, are also marked as bad pixels.

A bias frame was subtracted from all science data. Sky subtraction is done simply, using the GNSSKYSUB routine, by subtracting from each science frame a copy of itself, shifted by 21 binned pixels. This results in a positive-flux object spectrum in one half of the slit, and a negative-flux spectrum in the other half.

To generate a noise vector we use the same technique, but *add* the shifted images. This gives pixels, at the location of the galaxy, that include object flux and twice the sky flux, which is equal to the expected Poisson variance. We add to this twice the readnoise squared, to obtain the final variance spectrum.

Each sky-subtracted science image is then cleaned of cosmic rays, flat-fielded, and cut into individual slits. Corresponding arcs are extracted and wavelength calibrated; this calibration is then applied to each science frame. The four exposures are added, after applying a shift to account for the spectral dither and ignoring bad pixels identified in the bad pixel mask, which has been propagated through the same reduction procedures as the science frame. The same is done for the “noise” frame described above.

The negative-flux spectrum is then subtracted from its positive counterpart, for each spectrum, using by default a 3.5 pixel wide aperture (this is tweaked in a few cases, where necessary). A wavelength-dependent sensitivity function is determined by extracting the standard star spectrum, and comparing the flux to tab-

ulated values. This is applied to the final 1D and 2D object spectra, to give flux-calibrated spectra.

Our final step is to correct for telluric absorption. This is of particular importance since the H&K absorption lines in galaxies at our target redshift  $z \sim 0.95$  lie right on top of the A-band telluric line. We use our standard star observation to extract spectral regions around A-band ( $7500 < \lambda/\text{\AA} < 7700$ ) and B-band ( $6850 < \lambda/\text{\AA} < 6900$ ). A smooth continuum is subtracted, and we use the IRAF task TELLURIC to apply the correction to each spectrum according to the airmass in the image header.

### 2.3.4 Redshift Determination

Redshifts were measured by adapting the ZSPEC software, kindly provided by R. Yan, used by the DEEP2 redshift survey (Davis et al. 2003, 2007). This performs a cross-correlation on the 1D extracted spectra, using linear combinations of template spectra. The corresponding variance vectors described in § 2.3.3 are used to weight the cross-correlation.

We use templates of absorption line and emission line galaxies only, and for each galaxy ZSPEC returns a short list of possible redshifts, with associated  $\chi^2$  and  $R$  (Tonry & Davis 1979) values. Every spectrum is visually inspected, both in the 1D and 2D format. Particularly valuable is inspecting the 2D image prior to combining the positive- and negative-flux objects. Real emission lines are clearly identified by their dipole signature, and false peaks due to cosmic rays or other effects are easily removed. Generally, the 1D spectra are boxcar smoothed to  $\sim 10\text{\AA}$  pixels for visual inspection.

We adopt a simple, four-class method to quantify our redshift quality. Quality class 4 is assigned to galaxies with certain redshifts. Generally this is reserved for galaxies with multiple, robust features. With our (unbinned) spectral resolution, we are able to just resolve the [OII] doublet; in this case, a clear detection of the doublet alone would warrant a class 4 redshift. Quality class 3 are also very reliable redshifts, and we expect most of them to be correct. These include galaxies with a good match to Ca H&K for example, but no obvious corroborating feature. Similarly, single emission lines where a doublet is not convincing are generally assumed to be [OII] and given quality class 3. We would also use this in cases where H&K are detected in a region of telluric absorption, but there is at least one other likely match to an absorption feature. We take particular care not to assign class 3 or 4 to a galaxy for which H&K are the only identifiable features, and lie on a telluric absorption line.

Class 2 objects correspond to “possible” redshifts. These in-

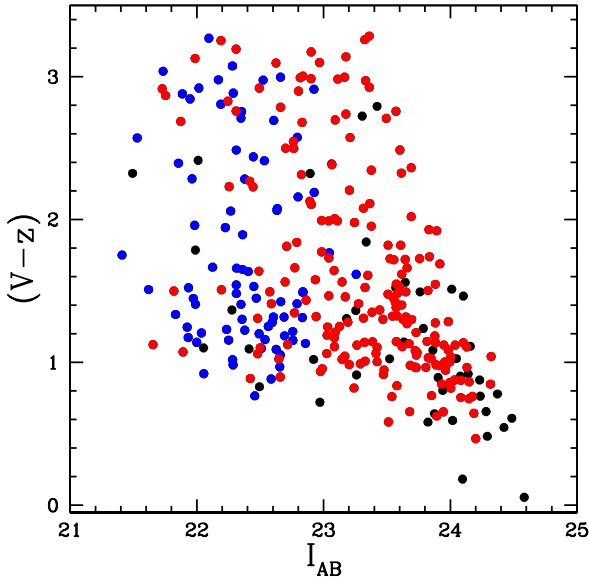


**Figure 1.** The colour-magnitude distribution for all galaxies with spectroscopy (from either GEEC or zCOSMOS) that lie within our GMOS fields, and have  $0.8 < z_{\text{phot}} < 1.5$ , within their  $1\sigma$  uncertainties. *Red points* represent GEEC targets with secure redshifts (quality 3 or 4), while *blue points* indicate secure zCOSMOS 10k redshifts (quality  $> 2$ ). The remaining, *black points*, are therefore those with a spectrum and  $0.8 < z_{\text{phot}} < 1.5$ , but without a secure redshift.

clude some spectra that are reasonably likely to be correct (e.g. H&K on top of a telluric line and no other corroborating features); but also some that are little more than guesses. Class 1 is reserved for “junk”, with no chance of obtaining a redshift.

In this analysis we only consider galaxies with class 3 or 4 quality redshifts.

## 2.4 zCOSMOS Observations and final catalogue

We also include in our analysis redshifts from the 10K release of zCOSMOS (Lilly et al. 2009). We include all galaxies with redshift quality greater than 2.0, which have a high probability ( $> 90$  per cent) of being correct (note the zCOSMOS quality flags are defined differently from our own). These provide a nice complement to our observations, by design, as they are restricted to the brighter galaxies that are not given priority in our target selection.

Figure 1 shows our final sample in colour-magnitude space. All optical colours and magnitudes are computed within a  $3''$  diameter aperture, on psf-matched images, as described in Capak et al. (2007). The galaxies plotted here are all those with an available spectrum, lying within our GMOS fields, and with  $0.8 < z_{\text{phot}} < 1$  within their  $1\sigma$  uncertainties. We choose the  $(V - z)$  colour as it brackets the  $4000\text{\AA}$  break at  $z \sim 0.95$ , and the  $I_{AB}$  magnitude for comparison with zCOSMOS. Red points represent GEEC targets with secure redshifts, while blue points indicate zCOSMOS 10k galaxies with secure redshifts. Distinct sequences of red and blue galaxies are apparent, and our redshift success rate is very high at all colours (see §3.1). Our GEEC spectra probe *red* galaxies up to 1.0 mag fainter than found in the 10k survey ( $I_{AB} < 22.5$ ), 0.65 mag fainter than DEEP2 (Cooper et al. 2008,  $r < 24.1$ ) and  $\sim 0.25$  mag fainter than EDisCS at this redshift (Halliday et al. 2004,  $I_{Vega} < 23$ , or  $I_{AB} \lesssim 23.3$ ). For blue galaxies we gain addi-

tional  $\sim 0.5$  mag depth relative to the  $I$ -selected zCOSMOS and EDisCS surveys.

## 3 ANALYSIS

### 3.1 Spectroscopic and Redshift completeness

We first consider the sampling completeness of our GMOS targets, defined as the fraction of potential targets for which we actually obtained a spectrum. Here, we define the complete sample to be all priority 1 galaxies (i.e. all  $21.5 < r < 24.75$  galaxies that have a photometric redshift within  $2\sigma$  of the estimated group redshift) that are within the GMOS field of view. Note that 100 per cent completeness in this sense could never have been achieved, because some of the field of view is permanently inaccessible due to the acquisition stars and, in a few cases, guider arm. We characterize our sampling completeness in terms of the IRAC  $[3.6\mu\text{m}]$  magnitude, since this is more closely related to galaxy stellar mass than the  $r$  band magnitude on which our selection was based. We include galaxies from the zCOSMOS 10K spectroscopic catalogue here as well, which mostly includes galaxies brighter than  $I_{AB} = 22.5$ . Although our target selection does not explicitly depend on galaxy colour, the reliance on photometric redshift uncertainty potentially introduces a colour-dependence. Thus we consider our sampling completeness as a function of both  $[3.6\mu\text{m}]$  magnitude and  $(V - z)$  colour. Specifically, we divide this colour-magnitude plane into several bins and calculate the completeness in each bin. For each colour bin we define a completeness function by fitting a line to the completeness as a function of  $[3.6\mu\text{m}]$  magnitude. We find that, regardless of how we do this, our completeness is remarkably uniform; it ranges from  $\sim 0.6$  to  $\sim 0.75$  with little dependence on colour or magnitude. This may be partly because the sample is too small yet to define the selection function with high enough precision, and we will revisit this when the survey is complete.

Another potential source of incompleteness is failure to obtain redshifts for targeted galaxies. We characterise our redshift success rate as a function of  $I_{AB}$  magnitude, since this corresponds most closely to the wavelength of features (like Ca H&K) commonly used for redshift identification at  $z \sim 0.9$ . This success rate, shown in Figure 2, is defined as the fraction of priority 1, targeted galaxies for which we obtained a redshift with quality 3 or 4. We find a remarkably high success rate of  $> 80$  per cent, for  $I_{AB} < 24$ . This is a testament in part to the high-quality spectra obtained at Gemini, and in particular the success of the nod & shuffle technique, which results in near-perfect sky subtraction in a spectral region dominated by sky emission lines. Moreover, we are helped by the exquisite photometric redshifts, which means our priority 1 list contains little contamination from higher redshift galaxies for which redshifts are difficult to obtain.

We show, as the blue points, the redshift success of the zCOSMOS 10k sample, restricted to the regions covered by our GMOS observations. Here the success rate is defined as the fraction of secure (quality  $> 2$ ) redshifts from all zCOSMOS targets within our GMOS fields of view. The success rate is also very high here,  $> 70$  per cent for  $I_{AB} < 22.5$ , which is their nominal completeness limit. We have also checked for a colour dependence on these success rates, and find no significant trend, as is visually apparent on Figure 1. Thus, both zCOSMOS and GEEC are highly successful at obtaining secure redshifts even for red, absorption-only galaxies. Many of these “failures” are in fact likely to be higher redshift galaxies, in which case they do not affect the success rate in our

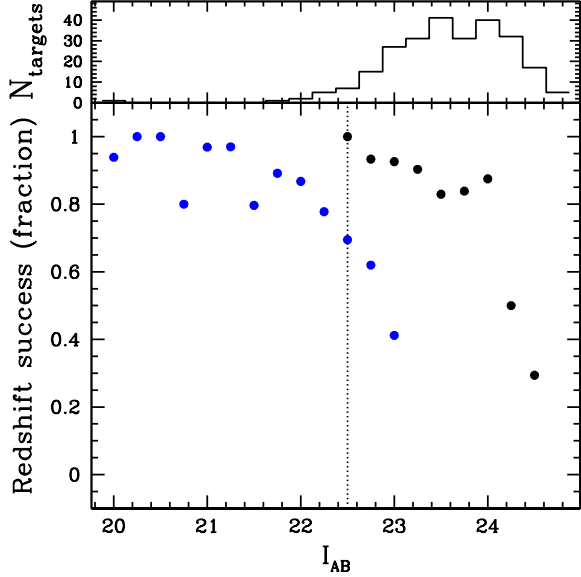


**Figure 2.** *Top:* The histogram shows the number of priority 1, GEEC spectra, as a function of  $I_{AB}$  magnitude. *Bottom:* The redshift success rate of GEEC, defined as the fraction of priority 1 galaxies with good (quality 3 or 4) redshifts, is shown as the black points. The blue points represent a similar quantity for the zCOSMOS 10k sample within our field; here it is the fraction of all galaxies in our GMOS fields with a zCOSMOS spectrum that have a redshift quality of  $> 2.0$ . The vertical, dotted line at  $I_{AB}$  represents the nominal, zCOSMOS completeness limit. With GEEC, we are highly complete for galaxies up to 1.5 mag fainter than this.

limited redshift range of interest. We therefore apply no further corrections for redshift incompleteness; the only weight comes from the sampling fraction.

In Figure 3 we compare our spectroscopic redshifts with the corresponding photometric redshift and its uncertainty. Red points represent secure redshifts for priority 1 galaxies in GEEC. These all, by definition, have a  $z_{\text{phot}}$  within  $2\sigma_{z_{\text{phot}}}$  of the group redshift ( $0.88 < z < 0.97$  for this sample). Effectively, this selects galaxies that either have  $z_{\text{phot}}$  close to the group redshift, or galaxies with poorly determined  $z_{\text{phot}}$ , which have large error bars. We see that not only do the spectroscopic and photometric redshifts agree very well, but that our preselection allows us to be efficient at targeting potential group members. The blue points represent secure redshifts in the zCOSMOS 10k sample.

During mask design, we preferentially target galaxies with photometric redshifts within  $2\sigma$  of the mean group redshift. Since we account for the uncertainty in  $z_{\text{phot}}$ , we do not expect to be strongly biased against galaxies for which  $z_{\text{phot}}$  is poorly determined due, for example, to a lack of strong features in the spectrum. However, we are potentially biased against “catastrophic failures”. To address this, in Figure 4 we show the difference between the spectroscopic and photometric redshift for all confirmed group members (see Section 3.3) with secure spectroscopic redshifts and  $0.7 < z_{\text{phot}} < 1.5$ , as a function of their  $(V - z)$  colour. Red points identify “priority 2” galaxies, which are those lower priority targets with  $z_{\text{phot}}$  more than  $2\sigma$  away from the group redshift. These make up only  $\sim 6$  per cent of the sample, with no measureable colour dependence. There is also no strong dependence on the quality of the spectroscopic redshift; the fraction of priority 2 galaxies that are actually group members is similar amongst quality 3 and quality 4

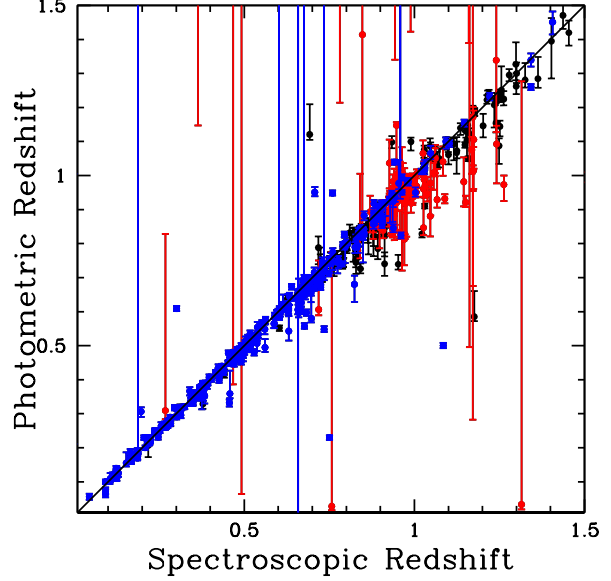


**Figure 3.** Spectroscopic redshifts are compared with photometric redshifts and their uncertainties. All galaxies with a secure redshift are shown. *Red points* are those GEEC galaxies with priority 1, which are those that have  $z_{\text{phot}}$  within  $2\sigma$  of the group redshift; *black points* represent GEEC galaxies with lower priority. *Blue points* are zCOSMOS 10k spectra within the same fields. Our spectra greatly increase the completeness and depth of the 10k survey at the redshift of these groups.

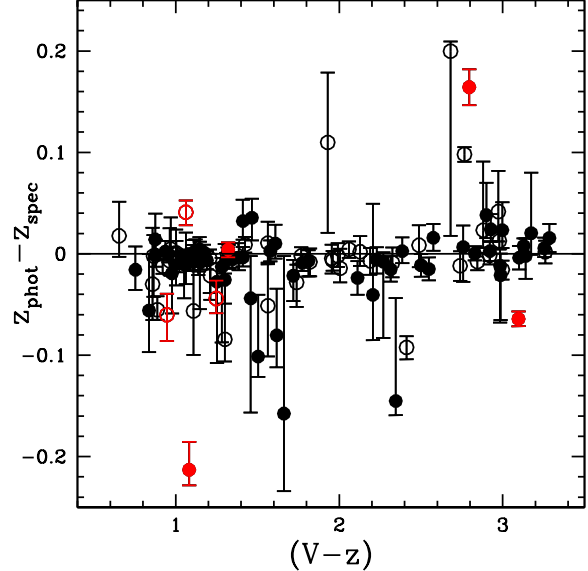


**Figure 4.** For confirmed group members with  $0.7 < z_{\text{phot}} < 1.5$  we show the difference between spectroscopic and photometric redshifts, as a function of  $(V - z)$  colour. Asymmetric errorbars are 68 per cent confidence intervals on  $z_{\text{phot}}$ . *Filled symbols* are quality class 4, which means the spectroscopic redshift is certain, while *open symbols* are class 3 and thus generally reliable (and used throughout this analysis). The *red points* identify those few group galaxies that were allocated lower priority during mask design because their  $z_{\text{phot}}$  is more than  $2\sigma$  away from the mean group redshift. These make up only  $\sim 6$  per cent of the total group population, with no obvious colour dependence.



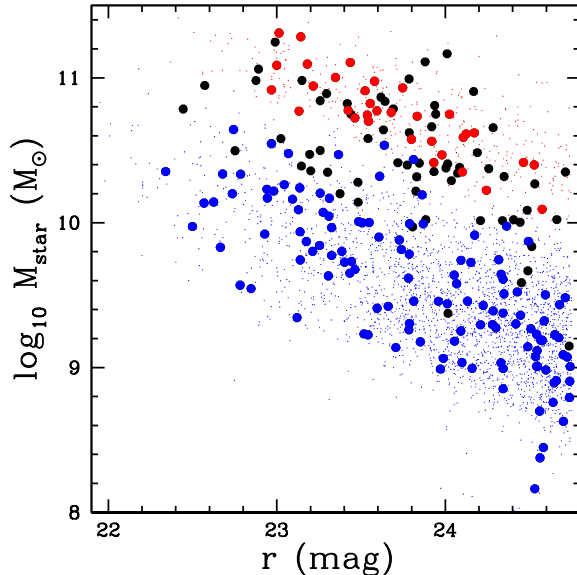


**Figure 5.** The stellar masses, computed for a Chabrier (2003) mass function and based on Bruzual & Charlot (2003) models, are shown as a function of  $r$  magnitude for a random subset of the photometric field sample (small points) and our spectroscopic sample (large, filled points), for  $0.8 < z < 1.0$ . The reddest galaxies,  $(V-z)^{0.9} > 2.7$ , are shown as red points, while the bluest galaxies  $(V-z)^{0.9} < 1.5$  are shown in blue (the remaining black points are those of intermediate colour). Our selection limit of  $r < 24.75$  imposes a colour-dependent mass limit, of  $M_{\text{star}} < 10^{10.1} M_{\odot}$  for red galaxies, and  $M_{\text{star}} < 10^{8.8} M_{\odot}$  for the bluest.

redshifts. We conclude therefore that our  $z_{\text{phot}}$  preselection does not introduce a large bias, though we will be able to test this more robustly at the end of the survey.

At this early stage of our survey, we have few duplicate observations with which to check our spectroscopic redshifts and determine a robust uncertainty. We do have eight good quality redshifts for galaxies that have an existing, good quality zCOSMOS redshift. From these, there appears to be a small bias in the sense that our redshifts are smaller by  $7.72 \times 10^{-4}$ , corresponding to a rest-frame velocity shift of  $\sim 120$  km/s at the redshift of interest. Although this should be treated as a preliminary offset, we correct our redshifts for it here. We use the same eight galaxies to estimate our redshift uncertainty and find  $\sigma_z \sim 4.1 \times 10^{-4}$ , corresponding to a rest-frame velocity uncertainty of  $\sim 65$  km/s at  $z = 0.9$ .

### 3.2 Stellar mass measurements and k-corrections

We fit the spectral energy distribution for each galaxy, using all available photometry, following the method described in McGee et al. (2010). Briefly, this is done by comparing with a very large grid of template Bruzual & Charlot (2003) models, covering a wide range of parameters, assuming a Chabrier (2003) mass function. The procedure is based on that of Salim et al. (2007), and assumes the star formation history of a galaxy can be represented by an exponential model with superposed bursts.

Stellar mass estimates are quite robust to the details of the fits, in part because of the availability of *Spitzer* IRAC data. The main assumptions that could lead to systematic errors are the initial mass function (IMF), the dust model (we use Charlot & Fall 2000), and the choice of galaxy evolution model. Of particular con-

cern could be the omission of thermally-pulsing AGB stars, which become increasingly important at higher redshifts (Maraston et al. 2006). This will be more relevant when considering comparison with  $z = 0$  observations, which we defer to after completion of the survey. For our purposes here, we are interested in comparing group galaxies with their field counterparts. Systematic effects like this on the mass estimates are not likely to be very different for the two populations. Thus we expect our conclusions to be robust to this and similar assumptions about IMF and dust geometry.

We k-correct all colours to  $z = 0.9$ , the redshift of interest for our survey, using the KCORRECT IDL software of Blanton & Roweis (2007). We denote these colours as, for example,  $(V-z)^{0.9}$ .

In Figure 5 we show our derived stellar masses as a function of  $r$  magnitude (our selection band), for both the photometric field sample (small points) and our spectroscopic sample, within  $0.8 < z < 1.0$ . The points are separated into the bluest galaxies,  $(V-z)^{0.9} < 1.5$ , and the reddest galaxies,  $(V-z)^{0.9} > 2.7$ . Our selection limit of  $r < 24.75$  implies we are 100 per cent complete above a mass limit of  $M_{\text{star}} \gtrsim 10^{10.5} M_{\odot}$ ; however, we are mostly complete for  $M_{\text{star}} \gtrsim 10^{10.1} M_{\odot}$ , missing only some of the reddest galaxies. We will therefore treat this as our nominal completeness limit throughout the paper. Note that the blue galaxies are complete for  $M_{\text{star}} \gtrsim 10^{9.6} M_{\odot}$ , and we probe masses as low as  $M_{\text{star}} \lesssim 10^{8.8} M_{\odot}$ .

### 3.3 Group masses and membership

For each group, we inspect the spatial and redshift distribution of the galaxies. Full results will be presented for all groups, after completion of the survey.

We start by considering all galaxies within  $r = 1$  Mpc of the nominal X-ray group centre from Finoguenov et al. (in prep). The velocity dispersion of these galaxies is determined using the gap-per estimate (Beers et al. 1990). We also compute the (unweighted) mean spatial position of the galaxies, and the *rms* projected separation from this centre, which we call  $R_{\text{rms}}$ . We then iterate this process, typically clipping galaxies with velocities  $> 1.5\sigma$  from the median redshift, and positions  $r > 2R_{\text{rms}}$  from the recomputed centre<sup>2</sup>. This converges after a few iterations, and we adopt the final  $\sigma$  and  $R_{\text{rms}}$ . Group members are then defined as those within  $3\sigma$  of the median redshift, and within  $2R_{\text{rms}}$  of the centre. Uncertainties on  $\sigma$  and  $R_{\text{rms}}$  are then computed using a jackknife method, iterating only over this list of group members. Thus, these uncertainties do not include systematic uncertainties due to the clipping process, which are likely to be at least  $\sim 15$  per cent (e.g. Wilman et al. 2005a).

We show how our sample compares with other, related surveys, in Figure 6. Points show the velocity dispersion of each group, as a function of redshift, for our present survey (filled circles), our previous GEEC sample at  $0.3 < z < 0.6$  (open triangles), and the EDISCS cluster and group sample Halliday et al. (2004); Poggianti et al. (2006, open circles). The median redshifts, velocity dispersions, and number of members in each of our groups is given in Table 1.

<sup>2</sup> The clipping parameters were tweaked for group 161, which is very close to group 150 in redshift and position. For this group we exclude galaxies with velocities  $> 1.4\sigma$  from the median redshift, and positions  $r > 1.6R_{\text{rms}}$  from the recomputed centre. The properties (dynamical and stellar mass) of this particular group are quite sensitive to this choice.

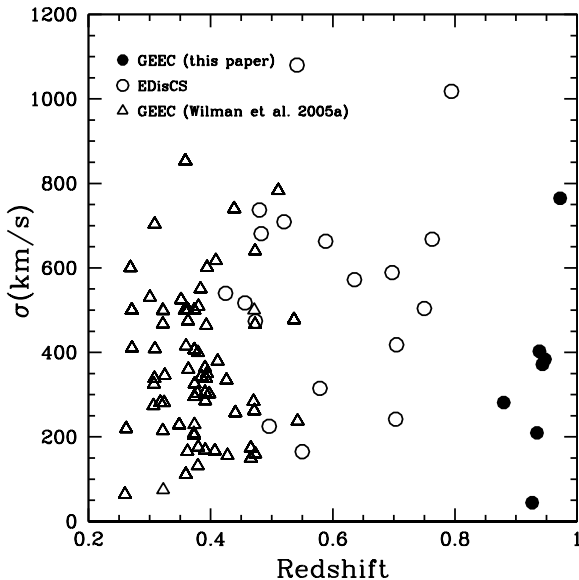


**Figure 6.** The velocity dispersion, as a function of redshift, for three samples of groups and clusters with high spectroscopic completeness. The present group sample is shown as *filled circles*, while our lower-redshift GEEC sample is shown with *open triangles*. The *open circles* represent the groups and clusters of the EDisCS survey (Halliday et al. 2004).

We estimate a dynamical mass, from the velocity dispersion  $\sigma$  and the radius  $R_{\text{rms}}$ ,

$$M_{\text{dyn}} = \frac{3}{G} R_{\text{rms}} \sigma^2. \quad (1)$$

The uncertainty is determined by propagating the jackknife uncertainties on  $\sigma$  and  $R_{\text{rms}}$ . The factor 3 in this equation is based on the assumption of isotropic orbits and an isothermal potential, but is only weakly dependent on those assumptions (Łokas & Mamon 2001).

Groups 150 and 161 are located within the same GMOS field. It is clear that group 161 is dynamically and spatially separated from group 150, but they are very close, separated by less than 1 Mpc and 1000 km/s (rest frame). Thus they may be part of the same, interacting system. The assignment of members to one group or the other is not entirely obvious, and our clipping algorithm was tuned to achieve a reasonable-looking separation.

Finally, the membership of group 213 is quite poor, and our completeness in this field is worse than elsewhere. We did, however, detect a serendipitous group (named 213a) at higher redshift,  $z = 0.9254$ . This group has six members, and a nominal velocity dispersion of only  $44 \pm 17$  km/s, rest frame — smaller than would be expected from redshift uncertainties alone, and likely dominated by systematic uncertainty. The group’s position is significantly offset from the X-ray detection, which is likely still correctly identified with the lower redshift system. We include both groups in our analysis; however, we do not attempt to determine a dynamical mass of group 213a since the velocity dispersion is clearly unresolved.

Our observations confirm that these are all low-mass systems, as expected from their X-ray fluxes. The dynamical masses of the targeted groups range from  $2.3 \pm 0.9 \times 10^{13} M_{\odot}$  to  $1.3 \pm 0.5 \times 10^{14} M_{\odot}$ .

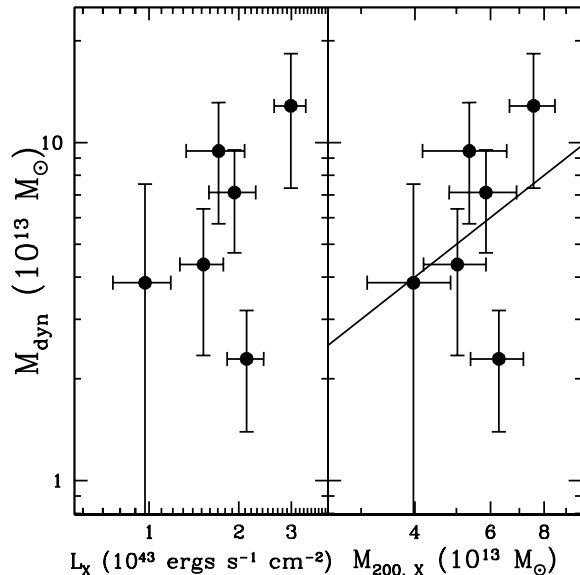


**Figure 7.** *Left:* The correlation between  $M_{\text{dyn}}$  and X-ray luminosity,  $L_X$ , is shown for the six targeted groups in our sample (i.e. excluding 213a, which is not detected in X-rays). *Right:* Here we show the same data, but as a function of  $M_{200,X}$  as determined directly from  $L_X$  assuming a scaling relation and calibrated from stacked weak lensing analysis (Leauthaud et al. 2010).

## 4 RESULTS

### 4.1 Dynamics and stellar fractions

With at least  $\sim 15$  spectroscopic members for most groups, we are able to make reasonable estimates of the dynamical mass, as described in § 3.3. In Figure 7 we compare these masses with the X-ray luminosity (left panel) and with the virial mass  $M_{200,X}$  estimated from this luminosity (right panel).  $M_{200,X}$  is estimated assuming a scaling relation and calibrated based on a stacked weak lensing analysis (Leauthaud et al. 2010).

The dynamical mass uncertainties are generally large, but the masses agree remarkably well with those estimated from the X-ray emission. The one outlier, which has a relatively low dynamical mass for its X-ray emission, is group 150; this group is close to and likely associated with 161. Its position on this plot is quite sensitive to the precise membership assigned; that is, the systematic uncertainty due to the choice of clipping parameters are likely dominant over the statistical uncertainties.

Total stellar masses can often be determined with much greater precision, with the dominant statistical noise term coming from the uncertainty in the radius  $R_{\text{rms}}$  within which the stellar mass is summed. The total stellar mass is computed over all galaxies in the sample; since we are incomplete for red galaxies with  $M < 10^{10.1} M_{\odot}$ , this is actually a lower limit. For the blue galaxies, about 75 per cent of the stellar mass is at  $M > 10^{10.1} M_{\odot}$ . Assuming this to be true for the red population as well, we estimate that our stellar masses underestimate the true total by less than 10 per cent. The statistical uncertainty is calculated from the jackknife uncertainties in  $R_{\text{rms}}$  and  $\sigma$ . In several cases, the group members with  $r < R_{\text{rms}}$  and  $|\Delta z| < 3\sigma$  do not change within the uncertainties on these quantities, which leads to a stellar mass estimate with, formally, zero uncertainty. We therefore impose an arbitrary, minimum uncertainty of 10 per cent on total stellar masses.



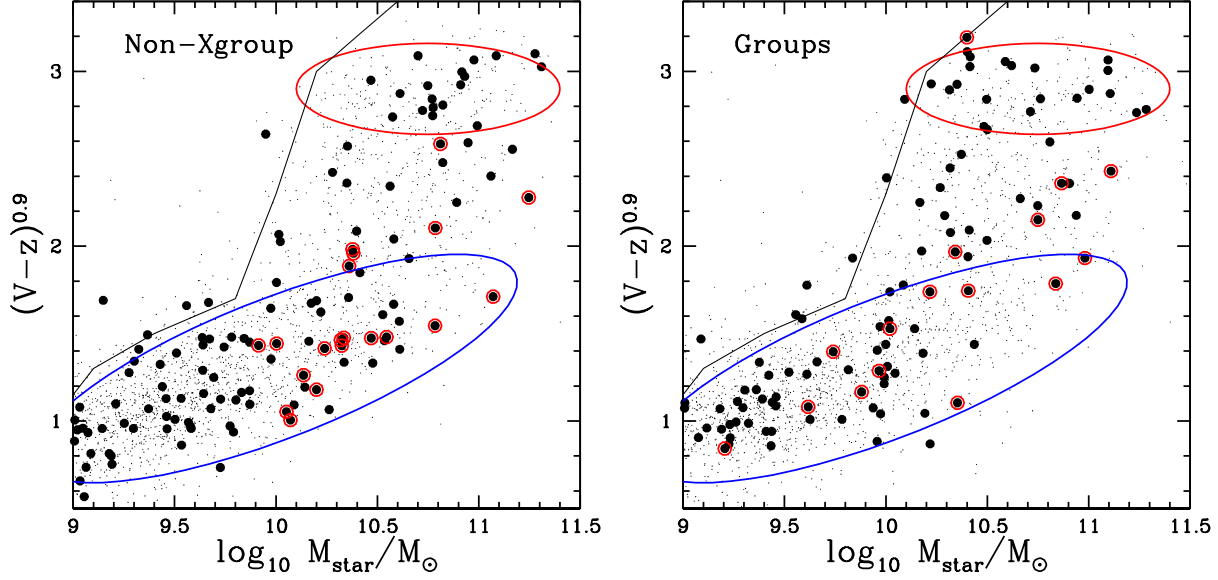


**Figure 9.** *Left:* The colours ( $k$ -corrected to  $z = 0.9$ ) and stellar masses of galaxies are shown for two samples. The small, black points are galaxies from the full COSMOS photometric catalogue, with  $r < 24.75$  and  $0.8 < z_{\text{phot}} < 1.0$ . We only show a random 10% of the points, for legibility. This represents the parent distribution from which our spectroscopic surveys (over a much smaller field) are drawn. The large, filled points represent galaxies with secure, spectroscopic redshifts at  $0.8 < z < 1$ , that lie within our GMOS fields but are not assigned to a group in our survey. We refer to these as “non-Xgroup” environment galaxies, to distinguish them from the general field (represented by the small points) which contains galaxies in all environments. The points circled in red indicate galaxies with  $24\mu\text{m}$  detections. Note the absence of low-mass, red-sequence galaxies in the non-Xgroup galaxies, and the dominance of the blue sequence for  $M_{\text{star}} < 10^{10.6} M_{\odot}$ . For illustration purposes only, the large red and blue ellipses approximately identify the “red sequence” and “blue cloud” populations. The solid line indicates our approximate completeness limit imposed by the  $r > 24.75$  selection. *Right:* The same, but now the filled points correspond to group members. Here, the faint end of the red sequence, visible in the parent photometric redshift catalogue, is filled in with confirmed group members. Moreover, there appears to be a prominent third population, that lies between the blue and red sequences at  $(V - z)^{0.9} \sim 2$ .

In Figure 8 we show the relationship between dynamical and stellar mass, for all six targeted groups. We exclude the serendipitous group 213a, since the velocity dispersion is unresolved; with only six members we cannot determine a reliable dynamical mass. For the remainder, the stellar fractions range from  $\sim 0.25$  per cent to  $\sim 3$  per cent, similar to what is observed both locally (e.g. Balogh et al. 2010) and at higher redshift (Giodini et al. 2009). The group with the highest stellar fraction is group 150 which, as mentioned previously, has a larger systematic uncertainty on its dynamical mass due to its close proximity to 161. The membership of group 161 itself is very sensitive to the choice of  $R_{\text{rms}}$ , and the uncertainty in this quantity leads to a large uncertainty in stellar mass. Thus, although there are hints of real diversity in the stellar fraction amongst our groups, the sample is too small at this time to draw any strong conclusions.

#### 4.2 Galaxy populations

Our main result from these first data is shown in Figure 9, as the correlation between  $(V - z)^{0.9}$  colour and stellar mass for the group and non-Xgroup samples. The small, black points represent galaxies in the entire COSMOS photometric redshift catalogue, within  $0.8 < z_{\text{phot}} < 1.0$  and restricted to  $r < 24.75$ , the GEEC selection limit. In the right panel, the large points correspond to spectroscopically confirmed group members, as defined in § 3.3. On the other hand, large points in the left panel represent all galaxies with secure redshifts  $0.8 < z_{\text{spec}} < 1$  that are unassociated with a group in our catalogue. We will refer to this spectroscopic sample as “non-Xgroup” galaxies, since they are confirmed non-members

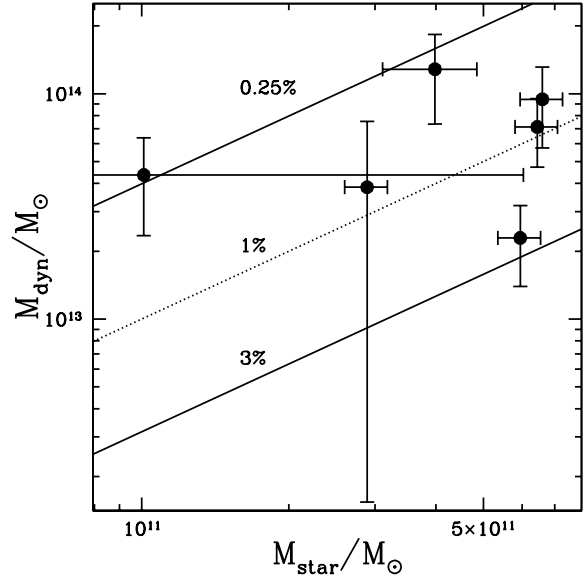


**Figure 8.** We show the measured dynamical mass as a function of total stellar mass, for each of our groups except the serendipitous group 213a. The stellar mass is the sum of all spectroscopically confirmed group members within a radius  $R_{\text{rms}}$ . The dotted line indicates a constant stellar fraction of 1 per cent; the solid lines on either side represent fractions of 0.25 per cent and 3 per cent, as indicated.

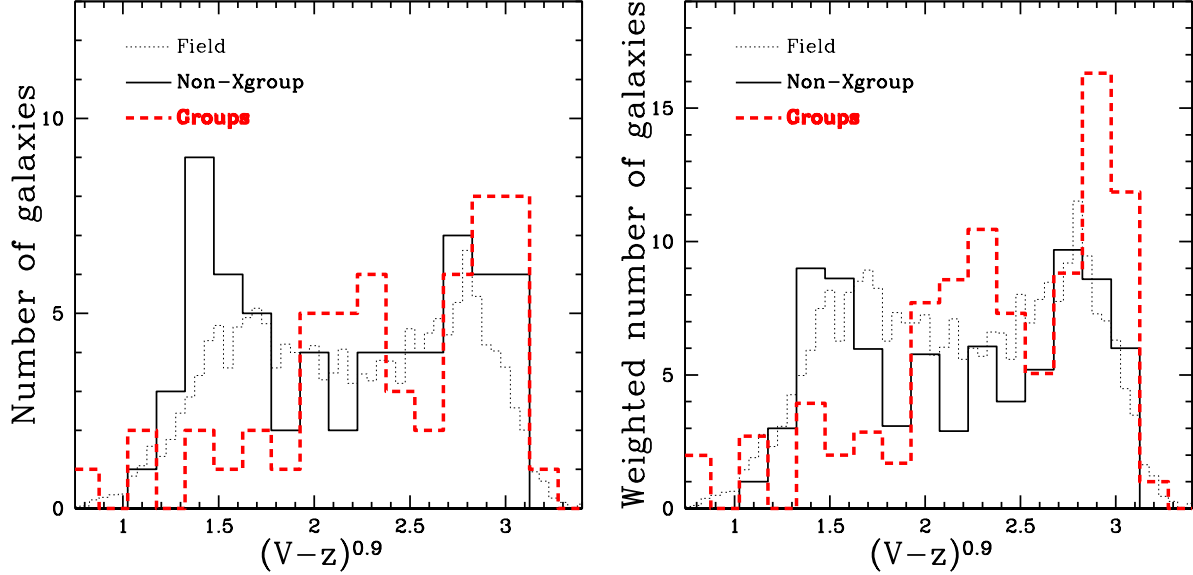


**Figure 10.** *Left:* The distribution of  $(V - z)^{0.9}$  colours are shown, for all galaxies with  $M_{\text{star}} > 10^{10.1} M_{\odot}$ . The *solid, black* line represents the distribution of our spectroscopic, non-group galaxy sample, which we suggest represents the “non-Xgroup” environment. It shows the well-known bimodal distribution, consisting of red and blue galaxy populations. The *red, dashed* histogram represents our spectroscopic group sample; there are few blue galaxies and, instead the population is dominated by red-sequence galaxies, and an apparently distinct population of intermediate-colour (“green”) galaxies. Finally, the *thin, dotted black* histogram is the distribution of all galaxies in COSMOS, with  $0.8 < z_{\text{phot}} < 1.0$ ,  $r < 24.75$  and  $M_{\text{star}} > 10^{10.1} M_{\odot}$ ; this has been renormalized to match the area of the red histogram. This represents the global, “field” population of galaxies. *Right:* The same, but where the group sample is now weighted for sampling incompleteness, and the COSMOS comparison sample is appropriately rescaled.

of our X-ray group sample. We cannot exclude the possibility that this sample still contains galaxies that are members of other groups, not identified in X-ray emission. The solid line in Figure 9 indicates our colour-dependent completeness limit, as a consequence of the  $r > 24.75$  mag selection. This is computed by simply looking at the average stellar mass of galaxies near the magnitude limit, as a function of colour.

We first note the usual structure in this colour-magnitude diagram, with a “red sequence” and “blue cloud” population. We show the approximate locations of these populations with red and blue ellipses, respectively. The red sequence in the groups is well populated at all masses above our completeness limit,  $M > 10^{10.1} M_{\odot}$ . In fact, there is some indication that the lowest-mass ( $M < 10^{10.5} M_{\odot}$ ), red galaxies appear *only* in groups, as they are absent in the “non-Xgroup” sample. However the sample is too small to be definitive about this, and we will defer a full analysis of the luminosity function shapes to the end of the survey.

The second interesting observation from Figure 9 is that the blue sequence appears to be very underpopulated amongst group galaxies, compared with the field, for  $M \gtrsim 10^{10.2} M_{\odot}$ . The blue galaxies that do exist here tend to lie at the red edge of the cloud; moreover, the “green valley” between the two sequences is well-populated, a point we will return to below.

We have matched our redshift catalogue with the deep *Spitzer* MIPS catalogue, which has a  $5\sigma$  detection limit of 0.071 mJy (Sanders et al. 2007). Using the calibration of Rieke et al. (2009), this limit corresponds to a star formation rate of  $\text{SFR} \sim 11.8 M_{\odot} \text{yr}^{-1}$  at  $z \sim 1$ . These  $24\mu\text{m}$  detections are circled in red in Figure 9. The non-Xgroup sample has a large population of massive, blue galaxies with  $24\mu\text{m}$  detections, indicating substantial star formation rates. In the groups, the massive  $24\mu\text{m}$  detections tend

to be considerably redder, populating the red envelope of the blue cloud, and the green valley itself.

The population of galaxies between the red and blue galaxies is of particular interest, as it may represent a transient phase. To explore this further, we show the distribution of colours, for all galaxies with  $M_{\text{star}} > 10^{10.1} M_{\odot}$ , in Figure 10. The black, solid histogram represents the distribution for our “non-Xgroup” spectroscopic sample; while the sample size is small, it shows the well-known bimodal distribution of colours, with a minimum around  $(V - z)^{0.9} \sim 2.3$ . This is statistically consistent<sup>3</sup> with the colour distribution of the full COSMOS “field” sample (for  $0.8 < z_{\text{phot}} < 1.0$ ) in the same stellar mass range, shown as the thin, dotted line. The red, dotted histogram represents our spectroscopic group sample. The left panel shows these data unweighted for completeness, while the right panel includes the completeness corrections. In both cases, the groups show a marked deficit of blue galaxies, while the intermediate-colour population is at least as abundant as in the general field.

Remarkably, the distribution suggests that this intermediate population may be distinct from both the red peak and blue cloud. Unfortunately the sample is not yet quite large enough to unambiguously identify these “green” galaxies with the group environment; a KS test on the unweighted distributions in Figure 9 confirms that the group distribution has a  $\sim 1$  per cent probability of being drawn from the same distribution as the parent, field population; or a  $\sim 2.5$  per cent chance of being drawn from the spectroscopic, “non-Xgroup” sample. It is also interesting that the “green” population (with  $1.9 < (V - z)^{0.9} < 2.4$ ) makes up a similar fraction of the total in the general field ( $\sim 25$  per cent) as in the groups

<sup>3</sup> A KS test shows there is a 38 per cent probability that the two distributions are drawn from the same parent population.

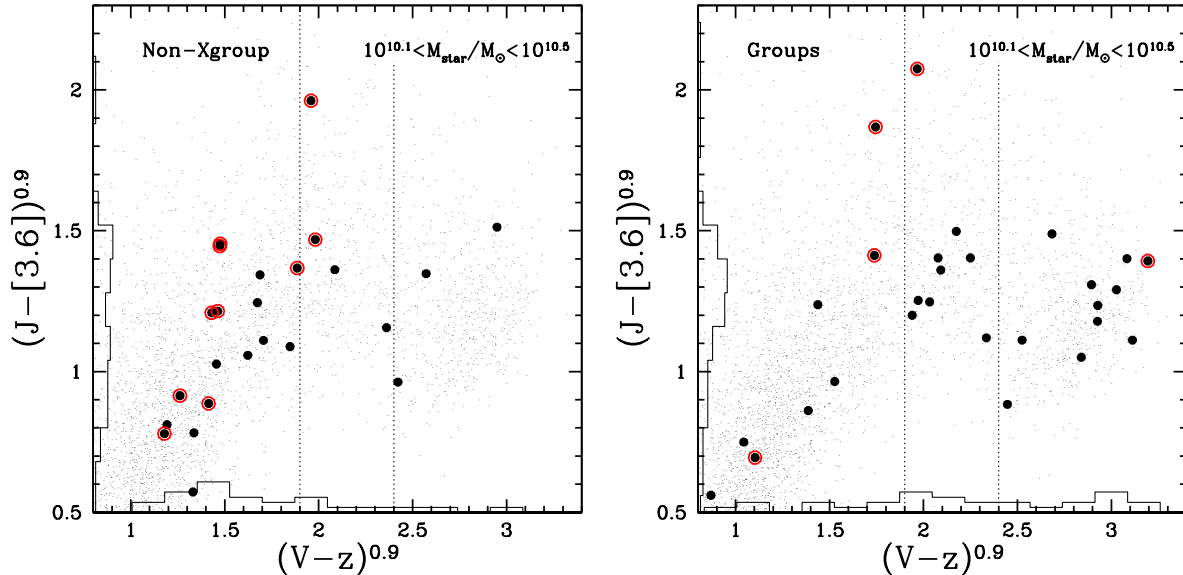


**Figure 11.** Colour-colour plots, aimed at separating dust-reddened spiral galaxies from the truly passive population (e.g. Balogh et al. 2009). The small, black points represent a random third of the COSMOS sample (limited to  $r < 24.75$ ), while the large points are our spectroscopically confirmed galaxies. Confirmed group members are shown in the *right* panel, while non-group members (the “non-Xgroup” spectroscopic sample) are shown on the *left*. In both cases, only galaxies with  $10^{10.1} < M_{\text{star}}/M_{\odot} < 10^{10.5}$  are shown. Points encircled in red represent those group members that are found in the deep MIPS source catalogue. With the exception of the single point near the top of the figure, none of the group galaxies in the apparently distinct population of “green” galaxies (between the dashed lines) have the red  $(J - [3.6])^{0.9}$  colours expected of dusty, star-forming galaxies. The histograms on either axis just represent the arbitrarily normalized distribution of each colour; the intermediate population is only apparent in colours that bracket the 4000Å break.

( $\sim 30$  per cent). The main difference between the two distributions is that, in the groups, the bluer peak contains only  $\sim 10$  per cent of the galaxies, while the fraction is  $\sim 35$  per cent in the field.

Whether or not it is unique to galaxy groups, the existence of this population of galaxies with intermediate colours is likely robust. Galaxies of this colour are found in all seven of our groups, and we have checked that the distribution in Figure 10 is not greatly affected by the k-corrections, redshift quality cut or group membership determination parameters. In Figure 11 we show colour-colour diagrams of our spectroscopic samples, again compared with the field sample from COSMOS. We show both the “non-Xgroup” spectroscopic sample, and the confirmed group members, in separate panels, and we restrict the plots to galaxies with  $10^{10.1} < M_{\text{star}}/M_{\odot} < 10^{10.5}$  to focus on the lowest-mass galaxies for which our sample is complete. The second colour here,  $(J - [3.6])^{0.9}$ , is chosen to sample approximately rest-frame  $(R - H)$ , a colour that should be sensitive to dust (e.g. Wolf et al. 2005; Balogh et al. 2009). Indeed, in the parent sample we can clearly see the star-forming (blue) sequence extends to red colours in  $(V - z)^{0.9}$ ; but they remain distinct from the passive population by virtue of their very red  $(J - [3.6])^{0.9}$  colours.

Interestingly, most of the “green” galaxies have relatively blue  $(J - [3.6])^{0.9}$  colours, suggesting that they are not exceptionally dusty. The only exception in the group population is the single galaxy near the top of the figure, which is in fact an edge-on spiral galaxy (see Fig 13 and later discussion). Interestingly, the distinct population of “intermediate” galaxies is not apparent in the  $(J - [3.6])^{0.9}$  distribution alone. We have checked using other filter combinations, and confirm that it is only apparent in colours that bracket the 4000Å break.

The matches to the deep MIPS catalogue are shown as red circles in Figure 11. Few of our group galaxies are detected; in

particular of the nine “green” galaxies in the mass range shown here, only one is detected at  $24\mu\text{m}$ . This is the edge-on, dusty spiral with very red  $(J - [3.6])^{0.9}$  colour noted previously. It has a  $24\mu\text{m}$  flux of  $\sim 0.24$  mJy which, using the calibration of Rieke et al. (2009), corresponds to a  $\text{SFR} \sim 78 M_{\odot} \text{yr}^{-1}$ .

With the full sample in hand, we will be able to combine spectra for galaxies with similar stellar masses and colours, to do a careful line strength analysis. For now, we have qualitatively checked the individual spectra of the confirmed group members which lie in this intermediate-colour region. About half of the galaxies show [OII] emission, although it is weak in all cases. Surprisingly, many of the galaxies have prominent  $\text{H}\delta$  absorption lines, and higher-order Balmer lines are also often apparent. This is intriguing and suggests these galaxies may be associated with the recent cessation of star formation (see also De Lucia et al. 2009; Yan et al. 2009). In particular, Poggianti et al. (2009) find that galaxies with strong  $\text{H}\delta$  absorption may be especially numerous in those groups in the EDisCS sample that have a low fraction of star-forming galaxies. We show six of the better-quality spectra, in Figure 12. The spectra have been deredshifted, and boxcar-smoothed over 11 pixels, corresponding to a rest-frame dispersion of  $5.2\text{\AA}$  per smoothed pixel. The bottom two spectra have strong absorption lines, including  $\text{H}\delta$ , and no significant [OII] emission. The next two show both emission and strong absorption lines, while the top two show an ordinary emission-line and absorption line galaxy. We will defer a quantitative analysis of these line indices to completion of the sample, where we can increase the signal-to-noise ratio by combining spectra for different classes of galaxies (Dressler et al. 2004).

Finally, we consider the morphologies of the spectroscopic group members, using the *HST* image cutouts shown in Figure 13. We just consider galaxies with  $10.1 < \log M_{\text{star}}/M_{\odot} < 10.5$  and secure redshifts, and divide them into blue ( $1.2 < (V - z)^{0.9} <$

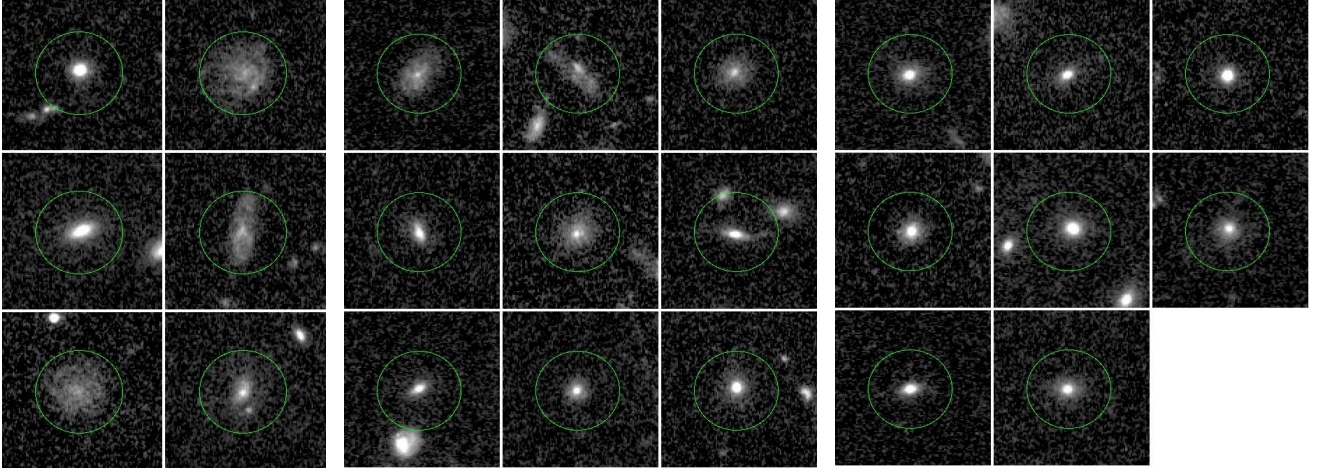


**Figure 13.** The *HST* F814W images of spectroscopically confirmed group galaxies in our sample, with  $10.1 < \log M_{\text{star}}/M_{\odot} < 10.5$ . The *left*, *middle* and *right* panels show blue, green and red galaxies respectively, as defined in the text. All images are 6.0 arcsec on each side (47 kpc at  $z = 0.9$ ), and the scales and colourbars are matched, with a square-root scaling applied. Colours are measured within a  $3''$  diameter aperture, indicated by the green circles. In each panel, galaxies are sorted by colour; galaxies get progressively redder moving left-to-right, top-to-bottom. The green galaxy population appears morphologically distinct from both the blue and red population. Most of them possess disks, though they are smaller and less structured than those of the blue population. The exception is the edge-on disk galaxy (top row, middle column), that is the MIPS-detected galaxy lying on the dusty star-forming sequence of Figure 11.

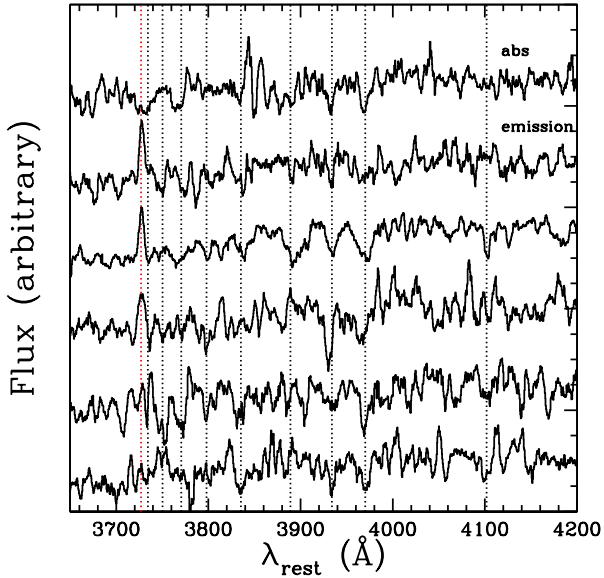


**Figure 12.** Selected spectra of “green”, spectroscopically confirmed group members. The spectra have been deredshifted, and smoothed. Vertical lines show the rest-frame wavelengths of common absorption lines (the Balmer series and Ca H&K), and of [OII] emission (3727 Å, in red). The four galaxies on the bottom have prominent high-order Balmer absorption lines, possibly indicative of recently truncated star formation.

1.9), green ( $1.9 < (V - z)^{0.9} < 2.5$ ) and red ( $2.7 < (V - z)^{0.9} < 3.2$ ) galaxies. We defer a detailed discussion, including surface-brightness profile fitting, to later papers based on the full sample. The images here are interesting even qualitatively, as the three populations appear to be morphologically distinct. The small blue population is fairly heterogeneous but includes three galaxies with large, structured disks, while the red galaxies are mostly simple elliptical galaxies with little disk component. The green galaxies are intermediate — in general, they are small, centrally concen-

trated, smooth and regular in appearance. Most appear to have disks, though none are as large or as structured as those found in the blue population. This tendency for intermediate-colour galaxies to have intermediate morphologies is also seen in the EDisCS sample at somewhat lower redshift Poggianti et al. (2008). The exception is an edge-on disk system, which is the MIPS-detected source, lying on the dusty-end of the blue-galaxy sequence in Figure 11. Excluding this galaxy, only one of the eight shows obvious signs of interaction with neighbours.

Thus, although this preliminary sample is small, there is evidence for a distinct galaxy population, with properties intermediate between the blue cloud and red sequence. It is prominent in our sample of groups and is in fact dominant over the blue cloud in the mass range  $10.1 < \log M_{\text{star}}/M_{\odot} < 10.5$ .

## 5 DISCUSSION AND CONCLUSIONS

We have presented first results from our ongoing Gemini spectroscopic survey of galaxy groups at  $z \sim 1$ . Using GMOS in nod & shuffle mode, with two hour exposures, we are able to obtain secure redshifts for galaxies up to 1.5 mag fainter than zCOSMOS, and thus obtain  $\gtrsim 10$  members per group with stellar masses  $M_{\text{star}} > 10^9 M_{\odot}$ . Our final sample will consist of  $\sim 20$  groups. Here we present the survey strategy, and first results on a sample of seven groups.

Our main discovery is that the groups host a population of “green” galaxies with colours and morphology that are intermediate between the usual blue cloud and red sequence. While a small fraction of these are dusty, edge-on spiral galaxies, most appear to be a truly intermediate population. Interestingly, most of the group population ( $\sim 90$  per cent) is made up of these green- and red-sequence galaxies; compared with the general field the groups are largely devoid of massive, blue galaxies.

The simplest explanation for the presence of these green galaxies is that they are transients. Broadly speaking there are two likely scenarios that might give rise to such a population. In the first hypothesis, they represent a normal phase of evolution in most, if



not all, galaxies. If galaxies form stars episodically, due to variations in cooling, accretion, and feedback processes, we might expect them to cycle between the blue and green (or red) population. In this case, the main characteristic of the group population is the lack of blue galaxies, which would suggest that it is the *rejuvenation* of star formation that has been halted. This is consistent with “strangulation” models, in which the normal star formation in disks of satellite galaxies is undisturbed, but the supply of fresh gas has been removed (e.g. Larson et al. 1980; Balogh et al. 2000).

Recently there have been indications that AGN inhabit the “green valley” of the galaxy colour distribution (e.g. Martin et al. 2007; Georgakakis et al. 2008; Cardamone et al. 2010), although this is somewhat controversial (Xue et al. 2010). This is tempting evidence that the onset of AGN feedback leads to the cessation of star formation, as predicted by models (e.g. Croton et al. 2006; Bower et al. 2006), and in support of our first hypothesis. Only one of our green, group members is detected as an X-ray point source; it is one of the more massive such galaxies, with  $M_{\text{star}} = 10^{10.66} M_{\odot}$ . Several of the more massive, green galaxies, with  $M_{\text{star}} > 10^{10.6} M_{\odot}$ , are detected at  $24\mu\text{m}$ , and thus may be candidates for obscured AGN (Georgakakis et al. 2008). However, few of the lower mass candidates are detected in the deep MIPS observations, and it is possible that they have a different origin.

The second hypothesis is that the dense environment of groups directly induces a decline in star formation rate (possibly preceded by a burst of star formation), that causes galaxies to migrate from the blue cloud to the red sequence. Recently, several studies of groups and clusters at this redshift have uncovered evidence of a galaxy population with specific star formation rates significantly different from surrounding field galaxies of the same stellar mass. In some cases this is seen as a reduced star formation rate (e.g. Vulcani et al. 2010), while in other cases there is an apparent *enhancement* of star formation (e.g. Elbaz et al. 2007; Muzzin et al. 2008; Cooper et al. 2008; Ideue et al. 2009; Li et al. 2010; Kocevski et al. 2010). Which effect dominates appears to depend both on stellar mass and local density (Sobral et al. 2010), but in any case this provides support for our second hypothesis. In this case, we would expect at least a subset of the green population to exist *only* in such environments and to have a spectral signature that is distinct from galaxies undergoing a “normal” cycle of star formation. Unfortunately, the present sample is not large enough to conclusively rule out the possibility that the intermediate “green” galaxies found in the GEEC groups are equally abundant in other, lower-density (or higher-density) environments. This should be possible with the final sample which, importantly, will include a larger sample of non-group galaxies with similar selection properties.

Assuming that the population of green galaxies represents a one-way transition between the blue and red populations, we can use their abundance in groups to estimate the timescale associated with this transition. We have therefore calculated some simple population synthesis models, using the Bruzual & Charlot (2003) code, with a Chabrier (2003) initial mass function and sub-solar metallicity ( $[\text{Fe}/\text{H}] = -0.33$ ). We assume a simple extinction model, with  $\tau_v = 1$ , with 30 per cent of the extinction arising from the ambient interstellar medium. Assuming galaxies form at  $z = 5$ , the maximum age for a galaxy at  $z = 0.9$  is about 5 Gyr. For our default models, we assume that the star formation rate is constant for the first 3 Gyr, after which it begins to decline exponentially with a timescale  $\tau$ . In Figure 14, we show the predicted  $(V - z)^{0.9}$  colour as a function of time after this decline begins, for  $\tau/\text{Gyr} = 0.1, 0.5, 1, 2$  and 3. In order to better match the colours

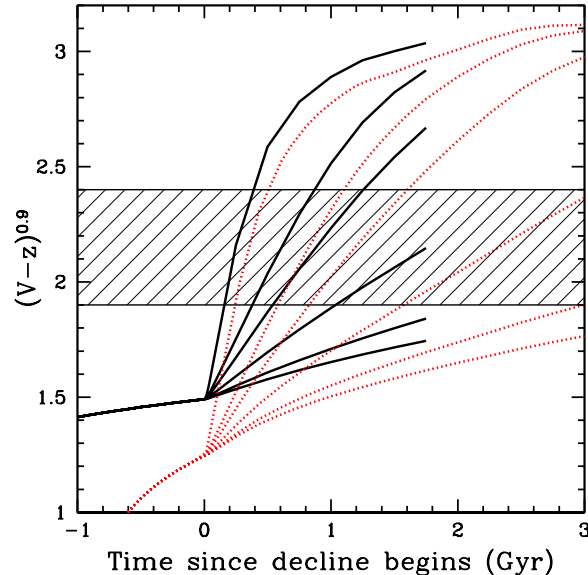


**Figure 14.** We show predictions of  $(V - z)^{0.9}$  colours, from a series of Bruzual & Charlot (2003) stellar population synthesis models, assuming a Chabrier (2003) IMF and  $[\text{Fe}/\text{H}] = -0.33$ . The black, solid lines represent models which have a constant star formation rate for 3 Gyr, then exponentially decline for another 2 Gyr, with an exponential timescale  $\tau$ . The choices of  $\tau/\text{Gyr}$  are, increasing from the top curve downward, 0.1, 0.33, 0.5, 1, 2 and 3. The red, dashed lines are similar models, but where only the first 1 Gyr are spent with constant SFR, and the exponential decline occurs for the remaining 4 Gyr. In both cases, the time  $t = 0$  is defined to be the time at which the exponential decline begins. The shaded region indicates the observed colour range of “green” galaxies, that lie between the red sequence and blue cloud. Most of the models pass through the “green”, shaded region, and in both cases models with  $\tau \sim 1 \text{ Gyr}$  spend a considerable fraction of their lifetime at this colour.

of the red and blue peaks we have applied a  $+0.2 \text{ mag}$  offset to the predicted colours. Specifically, after 3 Gyr of constant star formation all models begin with colours close to the peak of the observed blue galaxy distribution. Galaxies with swift declines ( $\tau < 1 \text{ Gyr}$ ) reach  $(V - z)^{0.9} \sim 3.1$ , the observed red peak.

We now turn our attention to the models which are able to reproduce the observed colours of the “green” population,  $1.9 < (V - z)^{0.9} < 2.4$ , indicated by the shaded region. Models with  $\tau > 1 \text{ Gyr}$  are effectively ruled out, as the galaxy never gets red enough to reach the green valley in the time allowed since  $z = 5$ . On the other hand, models with  $\tau < 0.5$  redden rapidly and spend little time in the green valley. To better quantify this, in Figure 15 we show the fraction of its 5 Gyr lifetime that these models spend in the green region, as a function of  $\tau$ . All models start in the blue cloud, with 3 Gyr of constant star formation, which means the maximum possible fraction of time as a green galaxy is 0.40. Interestingly, this picks out a particular timescale, of  $0.6 < \tau/\text{Gyr} < 1.3$ ; such models spend a significant fraction of time at this colour. In fact, this fraction compares reasonably well with the  $\sim 30$  per cent of galaxies observed at this colour.

Longer timescales can be accommodated if the truncation starts earlier. The red, dashed lines in Figure 14 show the results for models in which galaxies form stars at a constant rate for only 1 Gyr, before beginning their exponential decline. These galaxies start off much bluer, at  $(V - z)^{0.9} \sim 1.3$ ; otherwise their behaviour is qualitatively similar to those shown in Figure 14. The main difference

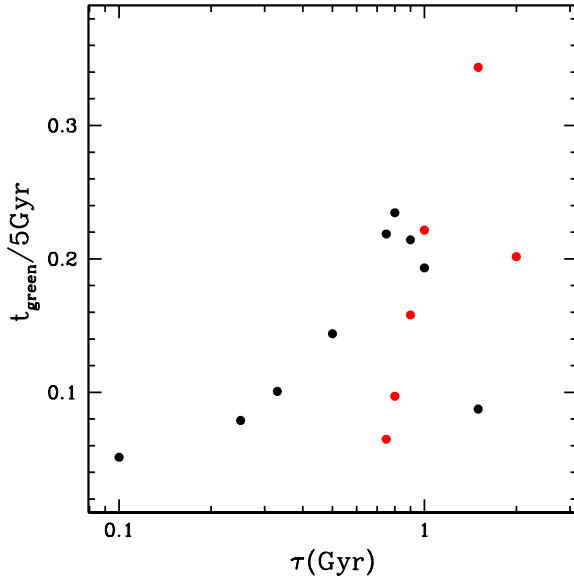


**Figure 15.** We show predictions from similar models as shown in Figure 14, with black points representing those that begin their decline after 3 Gyr of constant SFR, and red points those that decline after only 1 Gyr. In both cases, the total lifetime is 5 Gyr, as expected for a galaxy at  $z = 0.9$  that formed at  $z = 5$ . Each point shows the fraction of its lifetime (5 Gyr) that each model galaxy spends with “green” colours,  $1.9 < (V - z)^{0.9} < 2.4$ , as a function of  $\tau$ . For  $0.6 < \tau/\text{Gyr} < 2$ , these models spend more than 20 per cent of their lifetime as “green” galaxies, and thus represent a plausible interpretation of our data.

is they have up to 80 per cent of their lifetime available following the truncation. The red points in Figure 15 show the fraction of time these galaxies spend in the green region; in this case, longer timescales of  $\sim 2$  Gyr are preferred, and galaxies can spend up to 35 per cent of their life at this colour.

These are simplified, parametrized models. However, the results are encouraging as they demonstrate it is plausible for a significant fraction of galaxies to be observed in this special stage of evolution. If they really are migrating from the blue to the red sequence, it is unlikely that they are doing so with star formation rates declining much more rapidly than  $\tau \sim 0.6$  Gyr. Together with the undisturbed morphologies, this makes it unlikely that the transformation is being driven by mergers or rapid gas-depletion processes. Accelerated gas loss through a process like strangulation (e.g. Balogh et al. 2000; McCarthy et al. 2008) predicts a star formation rate decline on a timescale consistent with our observational constraints. This may be evidence that low-mass satellite galaxies have a fundamentally different evolution in groups, compared with their more massive counterparts, for which there is some evidence for merger-induced enhancements in star formation (e.g. Kocevski et al. 2010).

One of the next steps will be to couple the simple models presented here with an assembly history prediction (McGee et al. 2009) to achieve better constraints. Finally, with a larger sample of both group and isolated galaxies, and a comparison with more massive galaxy clusters at this redshift, we will be better able to determine to what extent these transforming galaxies are associated with the group environment.

## 6 ACKNOWLEDGMENTS

We thank the referee for a helpful report which led to the addition of several important clarifications and tests. We are also grateful to the COSMOS and zCOSMOS teams for making their excellent data products publicly available. This research is supported by NSERC Discovery grants to MLB and LCP. We thank the DEEP2 team, and Renbin Yan in particular for providing the ZSPEC software, and David Gilbank for helping us adapt this to our GMOS data.

## REFERENCES

- Baldry, I. K., Balogh, M. L., Bower, R. G., Glazebrook, K., Nichol, R. C., Bamford, S. P., & Budavari, T. 2006, *MNRAS*, 373, 469
- Balogh, M. L., Couch, W. J., Smail, I., Bower, R. G., & Glazebrook, K. 2002, *MNRAS*, 335, 10
- Balogh, M. L., Mazzotta, P., Bower, R. G., Eke, V., Bourdin, H., Lu, T., & Theuns, T. 2010, *MNRAS*, 1842
- Balogh, M. L., Morris, S. L., Yee, H. K. C., Carlberg, R. G., & Ellingson, E. 1997, *ApJL*, 488, L75+
- Balogh, M. L., Navarro, J. F., & Morris, S. L. 2000, *ApJ*, 540, 113
- Balogh, M. L., et al. 2004, *MNRAS*, 348, 1355
- . 2009, *MNRAS*, 398, 754
- Beers, T. C., Flynn, K., & Gebhardt, K. 1990, *AJ*, 100, 32
- Bell, E. F., Zheng, X. Z., Papovich, C., Borch, A., Wolf, C., & Meisenheimer, K. 2007, *ApJ*, 663, 834
- Blanton, M. R., & Roweis, S. 2007, *AJ*, 133, 734
- Bower, R. G., Benson, A. J., Malbon, R., Helly, J. C., Frenk, C. S., Baugh, C. M., Cole, S., & Lacey, C. G. 2006, *MNRAS*, 370, 645
- Bower, R. G., McCarthy, I. G., & Benson, A. J. 2008, *MNRAS*, 390, 1399
- Bruzual, G., & Charlot, S. 2003, *MNRAS*, 344, 1000
- Capak, P., et al. 2007, *ApJS*, 172, 99
- Cardamone, C. N., Urry, C. M., Schawinski, K., Treister, E., Brammer, G., & Gawiser, E. 2010, *ApJL*, 721, L38
- Chabrier, G. 2003, *PASP*, 115, 763
- Charlot, S., & Fall, S. M. 2000, *ApJ*, 539, 718
- Cooper, M. C., et al. 2008, *MNRAS*, 383, 1058
- . 2010, *MNRAS*, 409, 337
- Cowie, L. L., Songaila, A., Hu, E. M., & Cohen, J. G. 1996, *AJ*, 112, 839
- Croton, D. J., et al. 2006, *MNRAS*, 365, 11
- Cucciati, O., et al. 2010, *A&A*, 524, A2+
- Davis, M., et al. 2003, in Presented at the Society of Photo-Optical Instrumentation Engineers (SPIE) Conference, Vol. 4834, Society of Photo-Optical Instrumentation Engineers (SPIE) Conference Series, ed. P. Guhathakurta, 161–172
- Davis, M., et al. 2007, *ApJL*, 660, L1
- De Lucia, G., Poggianti, B. M., Halliday, C., Milvang-Jensen, B., Noll, S., Smail, I., & Zaritsky, D. 2009, *MNRAS*, 400, 68
- Dressler, A., Oemler, Jr., A., Poggianti, B. M., Smail, I., Trager, S., Sackett, S. A., Couch, W. J., & Ellis, R. S. 2004, *ApJ*, 617, 867
- Elbaz, D., et al. 2007, *A&A*, 468, 33
- Ellingson, E., Lin, H., Yee, H. K. C., & Carlberg, R. G. 2001, *ApJ*, 547, 609
- Elvis, M., et al. 2009, *ApJS*, 184, 158
- Finoguenov, A., et al. 2007, *ApJS*, 172, 182
- . 2009, *ApJ*, 704, 564
- . 2010, *MNRAS*, 403, 2063

- Font, A. S., et al. 2008, MNRAS, 389, 1619
- Georgakakis, A., et al. 2008, MNRAS, 385, 2049
- Gerke, B. F., et al. 2005, ApJ, 625, 6
- Gilbank, D. G., & Balogh, M. L. 2008, MNRAS, 385, L116
- Gilbank, D. G., et al. 2010, MNRAS, 405, 2419
- Giodini, S., et al. 2009, ApJ, 703, 982
- Glazebrook, K., & Bland-Hawthorn, J. 2001, PASP, 113, 197
- Gomez, P. L., Nichol, R. C., et al. 2003, ApJ, 584, 210
- Halliday, C., et al. 2004, A&A, 427, 397
- Hasinger, G., et al. 2007, ApJS, 172, 29
- Hopkins, A. M. 2004, ApJ, 615, 209
- Hou, A., Parker, L. C., Harris, W. E., & Wilman, D. J. 2009, ApJ, 702, 1199
- Ideue, Y., et al. 2009, ApJ, 700, 971
- Ilbert, O., et al. 2009, ApJ, 690, 1236
- Iovino, A., et al. 2010, A&A, 509, A40+
- Jeltema, T. E., et al. 2009, MNRAS, 399, 715
- Juneau, S., et al. 2005, ApJL, 619, L135
- Kawata, D., & Mulchaey, J. S. 2008, ApJL, 672, L103
- Knobel, C., et al. 2009, ApJ, 697, 1842
- Kocevski, D. D., et al. 2010, ArXiv e-prints
- Koopmann, R. A., & Kenney, J. D. P. 2004, ApJ, 613, 866
- Larson, R. B., Tinsley, B. M., & Caldwell, C. N. 1980, ApJ, 237, 692
- Leauthaud, A., et al. 2010, ApJ, 709, 97
- Lewis, I. J., et al. 2002, MNRAS, 333, 279
- Li, I., et al. 2010, MNRAS, in press, astro-ph/1010.1447
- Lilly, S. J., Le Fevre, O., Hammer, F., & Crampton, D. 1996, ApJL, 460, L1
- Lilly, S. J., et al. 2007, ApJS, 172, 70
- . 2009, ApJS, 184, 218
- Lokas, E. L., & Mamon, G. A. 2001, MNRAS, 321, 155
- Lu, T., Gilbank, D. G., Balogh, M. L., & Bognat, A. 2009, MNRAS, 399, 1858
- Maier, C., et al. 2009, ApJ, 694, 1099
- Maraston, C., Daddi, E., Renzini, A., Cimatti, A., Dickinson, M., Papovich, C., Pasquali, A., & Pirzkal, N. 2006, ApJ, 652, 85
- Martin, D. C., et al. 2007, ApJS, 173, 342
- McCarthy, I. G., Frenk, C. S., Font, A. S., Lacey, C. G., Bower, R. G., Mitchell, N. L., Balogh, M. L., & Theuns, T. 2008, MNRAS, 383, 593
- McGee, S. L., Balogh, M. L., Bower, R. G., Font, A. S., & McCarthy, I. G. 2009, MNRAS, 400, 937
- McGee, S. L., Balogh, M. L., Wilman, D. J., Bower, R. G., Mulchaey, J. S., Parker, L. C., & Oemler, Jr., A. 2010, ArXiv e-prints
- Moore, B., Katz, N., Lake, G., Dressler, A., & Oemler, A. 1996, Nature, 379, 613
- Muzzin, A., Wilson, G., Lacy, M., Yee, H. K. C., & Stanford, S. A. 2008, ApJ, 686, 966
- Noeske, K. G., et al. 2007, ApJL, 660, L43
- Noeske et al., K. G. 2007, ApJL, 660, L47
- Peng, Y., et al. 2010, ApJ, 721, 193
- Poggianti, B., et al. 2006, ApJ, 642, 188
- Poggianti, B. M., Smail, I., Dressler, A., Couch, W. J., Barger, A. J., Butcher, H., Ellis, R. S., & Oemler, A. J. 1999, ApJ, 518, 576
- Poggianti, B. M., et al. 2008, ApJ, 684, 888
- . 2009, ApJ, 693, 112
- Quilis, V., Moore, B., & Bower, R. 2000, Science, 288, 1617
- Rieke, G. H., Alonso-Herrero, A., Weiner, B. J., Pérez-González, P. G., Blaylock, M., Donley, J. L., & Marcillac, D. 2009, ApJ, 692, 556
- Rykoff, E. S., et al. 2008, MNRAS, 387, L28
- Salim, S., et al. 2007, ApJS, 173, 267
- Sanders, D. B., et al. 2007, ApJS, 172, 86
- Scoville, N., et al. 2007a, ApJS, 172, 38
- . 2007b, ApJS, 172, 1
- Skibba, R. A., & Sheth, R. K. 2009, MNRAS, 392, 1080
- Sobral, D., Best, P., Smail, I., Geach, J., Cirasuolo, M., Garn, T., & Dalton, G. B. 2010, MNRAS, 1657
- Tonry, J., & Davis, M. 1979, AJ, 84, 1511
- Vulcani, B., Poggianti, B. M., Finn, R. A., Rudnick, G., Desai, V., & Bamford, S. 2010, ApJL, 710, L1
- Weinmann, S. M., van den Bosch, F. C., Yang, X., & Mo, H. J. 2006, MNRAS, 366, 2
- Wilman, D. J., Balogh, M. L., Bower, R. G., Mulchaey, J. S., Oemler, A., Carlberg, R. G., Morris, S. L., & Whitaker, R. J. 2005a, MNRAS, 358, 71
- Wilman, D. J., et al. 2005b, MNRAS, 358, 88
- Wolf, C., Gray, M. E., & Meisenheimer, K. 2005, A&A, 443, 435
- Xue, Y. Q., et al. 2010, ApJ, 720, 368
- Yan, R., et al. 2009, MNRAS, 398, 735